Special Issue

Optical Coherence Tomography for Retinal Surgery: Perioperative Analysis to Real-Time Four-Dimensional Image-Guided Surgery

Oscar M. Carrasco-Zevallos,[1] Brenton Keller,[1] Christian Viehland,[1] Liangbo Shen,[1] Michael I. Seider,[2] Joseph A. Izatt,[1,2] and Cynthia A. Toth[1,2]

[1]Department of Biomedical Engineering, Duke University, Durham, North Carolina, United States
[2]Department of Ophthalmology, Duke University Medical Center, Durham, North Carolina, United States

Correspondence: Cynthia A. Toth, Duke Eye Center, Box 3802, Durham, NC 27710, USA; cynthia.toth@duke.edu.

Submitted: February 5, 2016
Accepted: May 7, 2016

Citation: Carrasco-Zevallos OM, Keller B, Viehland C, et al. Optical coherence tomography for retinal surgery: perioperative analysis to real-time four-dimensional image-guided surgery. *Invest Ophthalmol Vis Sci*. 2016;57:OCT37–OCT50. DOI: 10.1167/iovs.16-19277

Magnification of the surgical field using the operating microscope facilitated profound innovations in retinal surgery in the 1970s, such as pars plana vitrectomy. Although surgical instrumentation and illumination techniques are continually developing, the operating microscope for vitreoretinal procedures has remained essentially unchanged and currently limits the surgeon's depth perception and assessment of subtle microanatomy. Optical coherence tomography (OCT) has revolutionized clinical management of retinal pathology, and its introduction into the operating suite may have a similar impact on surgical visualization and treatment. In this article, we review the evolution of OCT for retinal surgery, from perioperative analysis to live volumetric (four-dimensional, 4D) image-guided surgery. We begin by briefly addressing the benefits and limitations of the operating microscope, the progression of OCT technology, and OCT applications in clinical/perioperative retinal imaging. Next, we review intraoperative OCT (iOCT) applications using handheld probes during surgical pauses, two-dimensional (2D) microscope-integrated OCT (MIOCT) of live surgery, and volumetric MIOCT of live surgery. The iOCT discussion focuses on technological advancements, applications during human retinal surgery, translational difficulties and limitations, and future directions.

Keywords: intraoperative imaging, optical coherence tomography, vitreoretinal surgery

Lens-based magnification during slit-lamp examination is the cornerstone of retinal diagnostics. The concept of magnification was introduced during ocular surgery in 1946[1] in the form of the operating microscope, but it was not until seminal publications in 1967[2,3] that its widespread applicability in the field was ensured. In these early applications, the operating microscope was used primarily to improve the precision and repeatability of current surgical techniques. The subsequent development of pars plana vitrectomy (PPV)[4]—facilitated by improved surgical visualization afforded by the operating microscope[5]—was the key advancement that galvanized a revolution in posterior eye surgery. What followed were innovations in instrumentation[6] and illumination[7] along with increased automation of the operating microscope.[8] While instrumentation development is still ongoing,[9,10] the integration of noncontact indirect ophthalmoscopy into the operating microscope for wide-angle viewing in 1987[11] was the last major advancement in retinal surgical visualization.

When operating through a modern microscope, the surgeon is limited to an en face view, and axial information must be inferred from instrument shadowing and other indirect cues. However, retinal surgery requires precise three-dimensional (3D) manipulation of delicate tissue on the submillimeter scale. The introduction of an imaging modality that is superior or complementary to the operating microscope could dramatically enhance surgical visual feedback, help refine current techniques, and catalyze the development of novel procedures that rely on tomographic guidance.

Optical Coherence Tomography in Ophthalmology

Optical coherence tomography (OCT) is a noncontact tomographic imaging modality that achieves micrometer-scale axial resolution via interferometric detection of backscattered near-infrared light. Optical coherence tomography technology has dramatically improved since its inception in 1991,[12] and imaging speeds have progressed from real-time A-scans, to real-time B-scans,[13,14] to real-time volumes.[15,16] The advent of Fourier-domain OCT technology—in the form of spectral-domain OCT (SD-OCT) and swept-source OCT (SS-OCT)—resulted in improved sensitivity[17] and increased system robustness, which facilitated commercialization and led to widespread clinical adoption.

The imaging depth, resolution, and sensitivity of OCT are ideal for imaging transparent ocular structures and provide diagnostic potential similar to that of histologic analysis.[18,19] In vivo OCT retinal imaging was first demonstrated in 1993[20] and led to a revolution in the diagnosis and monitoring of many retinal pathologies.[21–24] Since then, OCT has been extended to a wide variety of applications, including specific retinal layer thickness analysis to derive disease indicators,[25–29] wide field-of-view imaging for evaluation of the retinal periphery,[30,31] motion-compensated in vivo imaging,[32,33] and retinal angiography without the need for exogenous contrast agents.[34–39]

Perioperative OCT

Motivated by its diagnostic potential, ophthalmic surgeons implemented OCT for perioperative analysis of retinal surgery in the mid-1990s.[40] Optical coherence tomography has since become an irreplaceable tool in preoperative surgical planning and postoperative monitoring of recovery, primarily because of its ability to image pathologic structures and surgically induced alterations that are difficult to detect with fundus photography.[41–43] Applications of perioperative OCT include localization and characterization of epiretinal membranes (ERM) during surgical planning, and confirmation of their removal or discovery of persistent ERM postoperatively.[44,45] Optical coherence tomography also enhanced monitoring of macular hole closure in the early postoperative period,[46,47] during which fundus photography was limited by opacity secondary to intravitreal gas and/or postvitrectomy debris. Additionally, OCT allowed correlation of macular hole size to closure rate,[48] as well as monitoring of ellipsoid zone (inner segment–outer segment [IS/OS] junction) deformation due to surgery,[49] and is considered the gold standard for differentiating full-thickness macular holes from lamellar holes.[50] Other studies demonstrated the increased sensitivity of OCT compared to fundus photography in diagnosing vitreoretinal adhesions,[43,51] diabetic macular edema,[51,52] and myopic foveoschisis, and retinal detachment.[53,54]

While OCT has clearly improved pre- and postoperative analysis, absence of this enhanced feedback during surgery limits the determination of surgical endpoints that may be visible on OCT. As a result, additional surgery is often required to repair persistent lesions or remove persisting tissue identified on postoperative OCT.[55] Because multiple surgical interventions are expensive and increase the patient's risk for adverse events, the next logical evolution in OCT management of retinal surgery was intraoperative OCT (iOCT). Early attempts to translate OCT into the operating suite demonstrated successful imaging of excised tumors,[56] postmortem specimens,[57] in vitro human arteries and nerves,[58] and structural alterations due to laser surgery.[59,60] Nevertheless, these early applications were confounded by time-domain technology—resulting in suboptimal imaging speeds and sensitivity—and their inability to image in vivo human surgery.

Handheld OCT During Surgical Pauses

Technological Development

Retinal iOCT was first accomplished using handheld OCT (HHOCT) probes during pauses in surgery. Handheld OCT technology was developed around the turn of the century[61,62] and successfully applied for pediatric imaging[55,63–66] using a commercial handheld SD-OCT system introduced in 2007 (Bioptigen, Inc., Research Triangle Park, NC, USA). The Bioptigen HHOCT featured a compact handheld imaging probe connected via flexible optical fiber to a portable cart (Fig. 1). The SD-OCT engine operated at 840 nm to produce tomograms with 5-μm axial resolution at 17k A-scans per second, and could readily achieve video-rate B-scans with minimal motion artifacts. This imaging speed represented a substantial improvement over time-domain OCT but still limited the volumetric acquisition time to several seconds. To acquire retinal images, the probe was positioned ~2 cm away from the patient's cornea and could be angled to center the scans on the site of interest. Optical coherence tomography data were visualized intraoperatively as B-scans and en face retinal images (also known as summed voxel projections [SVP]) displayed on a computer screen. Most importantly, unlike conventional tabletop scanners that required an upright and cooperative patient, HHOCT enabled imaging of supine patients and was readily applicable for intraoperative imaging during surgical pauses. Similar HHOCT systems from other vendors have since been developed and applied during macular surgery.[67–69]

Intraoperative Applications

Dayani et al.[70] at the Duke University Medical Center first demonstrated retinal iOCT imaging with HHOCT during surgical pauses in 2009. Indications for PPV in this study included macular hole, ERM, and vitreomacular traction (VMT). Static imaging was performed preincision and intraoperatively. Preincision iOCT images confirmed the disease of interest in all tested cases, while intraoperative images acquired immediately after ERM and internal limiting membrane (ILM) peeling revealed alterations in the retinal contour and decrease in macular hole size compared to the preincision images. Moreover, residual ILM was discovered with HHOCT intraoperatively, confirming to the surgeons the need for additional peeling. Despite its small sample size, this seminal study demonstrated the feasibility of iOCT with HHOCT to alter surgical decision making. Subsequent studies used intraoperative HHOCT to assess macular hole closure after ILM peeling in a pediatric case[71] and to evaluate retinoschisis during treatment of optic pit–related maculopathy.[72] Handheld OCT systems were also employed to differentiate Coat's disease from diffuse retinoblastoma intraoperatively,[73] and to study the inner retinal surface after peeling of ERM "with connecting strands" and their correlation to outcomes following ILM peeling.[74]

To increase imaging stability, Ray et al.[75] secured an HHOCT probe to the operating microscope using a custom mount and successfully imaged 25 consecutive eyes undergoing retinal surgery. The microscope-mounted approach was also adopted by the Cleveland Clinic Cole Eye Institute for the 2-year PIONEER study.[76] This study comprised 256 eyes undergoing retinal surgery for a variety of indications, making it the largest evaluation of intraoperative HHOCT to date. The most common indications for surgery were ERM and macular hole. The authors reported that in 63 out of 146 procedures involving ERM peeling, iOCT impacted surgical decision making, with confirmation of peeling completion being the most commonly reported impact. Other results from the PIONEER study included quantification of macular hole volumetric alterations before and after ILM peeling in 21 consecutive eyes, in which increased macular hole volume and increased height between the ellipsoid zone (IS/OS junction) and RPE were reported.[77] The latter finding in particular was interpreted by the authors as potentially implying that photoreceptor stretching had occurred during surgery. In the same study, iOCT also revealed full-thickness macular hole development after hyaloid elevation during surgeries for VMT,[78] persistent subretinal fluid and significant alterations to foveal architecture during surgeries for rhegmatogenous retinal detachment,[79] and significant membrane peeling–induced retinal alterations with both intraocular forceps and membrane scrapers.[80]

Translational Difficulties and Limitations

As originally reported in 2009 by Dayani et al.,[70] intraoperative HHOCT imaging was performed by placing several fingers on the patient's forehead to stabilize the probe. A learning curve for localizing regions of interest and obtaining high-quality images was noted due to challenges in manual alignment and potential instability of the imager's hand. The custom mount developed by Ray et al.[75] exploited the microscope's motorized X/Y/Z translation to facilitate alignment of the HHOCT

Investigative Ophthalmology & Visual Science

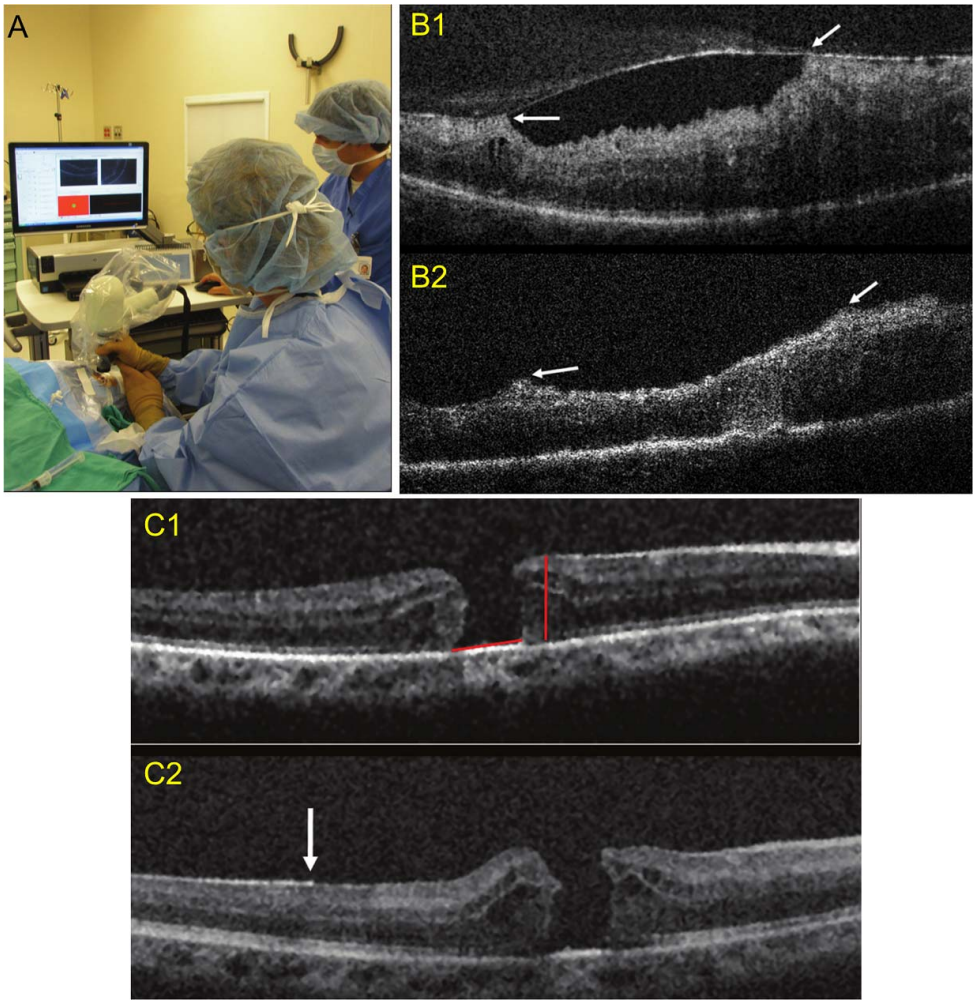

Figure 1. Handheld OCT (HHOCT) imaging during surgical pauses. (**A**) The surgeon holds the probe over the patient's eye and manually aligns the scan to the site of interest. Intraoperative HHOCT imaging requires displacement of the surgical microscope. (**B**) Intraoperative HHOCT before (**B1**) and after (**B2**) epiretinal membrane (ERM) peeling. Note the multiple ERM attachment points (*white arrows*) in (**B1**) and decreased retinal traction (*white arrows*) in (**B2**) with normalization of the retinal contour. (**C**) Preoperative (**C1**) and intraoperative HHOCT imaging immediately after internal limiting membrane (ILM) peeling (**C2**) in macular hole surgery. The postpeeling scan (**C2**) shows the elevated appearance of the hole edge and smaller base diameter, suggesting reduced traction. Residual ILM (*white arrow*) is also visible in (**C2**) as distinct hyperreflectivity along the retinal surface. Figures reprinted with permission from Dayani PN, Maldonado R, Farsiu S, Toth CA. Intraoperative use of handheld spectral domain optical coherence tomography imaging in macular surgery. *Retina*. 2009;29:1457–1468. © 2009 The Ophthalmic Communications Society, Inc.[70]

probe to the patient. However, in the microscope-mounted approach, the probe could not be offset angularly relative to the ocular pupil to image the retinal periphery. More importantly, the primary drawback of intraoperative HHOCT—in both the handheld and microscope-mounted approaches—was its restriction to surgical pauses since the microscope must be displaced away from the patient during imaging. Although these pauses could be relatively short—Dayani et al.[70] reported 4 to 5 minutes per imaging session and Ehlers et al.[76] reported 3.4 minutes per session—intraoperative HHOCT could not image the live instrument–tissue interactions that resulted in the structural alterations described above.

Live Two-Dimensional (2D) OCT Imaging of Surgery

Technological Development

The first demonstration of microscope-integrated OCT (MIOCT) to achieve concurrent microscope and OCT imaging of human retina was published by Tao et al. in 2010[81] at Duke University. The authors constructed custom optomechanics that allowed integration of a research OCT sample arm into a commercial operating microscope. The two modalities were coaligned with a dichroic mirror prior to the microscope objective to keep the microscope's working distance and surgeon's view unobstructed. Moreover, the coalignment allowed the microscope and OCT to focus at the same plane so that high-quality OCT images of structures in the focal plane of the operating microscope could be readily acquired. The MIOCT system was also compatible with the binocular indirect ophthalmic microscope (BIOM; Oculus Surgical, Inc., Port St. Lucie, FL, USA) for wide-field imaging of retinal surgery. The OCT beam was magnified prior to the microscope objective and BIOM to achieve a 2.5-mm beam diameter prior to cornea and 10-μm lateral resolution at the retina. Acquired OCT images were displayed on a computer monitor or wall-mounted display for surgical feedback.

Alternative MIOCT approaches include integration of the OCT sample arm at the microscope's surgical camera port to minimize microscope height,[82,83] the use of reflective ele-

ments and a tunable-focus lens to optimize OCT image quality,[84] and the incorporation of a microscope-integrated monocular heads-up display unit (HUD).[84,85] The latter development was particularly important since it allowed concurrent OCT and operating microscope visualization through the microscope oculars to facilitate real-time feedback to the surgeon.

All aforementioned MIOCT systems employed commercially available SD-OCT technology for intraoperative data acquisition and visualization.[86,87] While volumetric OCT data could technically be acquired with these systems, volume acquisition was slow (2–10 seconds) and rendering was restricted to post processing. Real-time volumetric imaging of retinal surgery was thus unfeasible and iOCT feedback was limited to 2D formats (B-scan and SVP).

We note that early MIOCT publications used the term "microscope-mounted OCT" to describe their systems.[81,88] This nomenclature was subsequently modified to MIOCT to better reflect the incorporation of the OCT into the operating microscope, and to differentiate it from microscope-mounted HHOCT devices described previously.

Surgical Applications

Comprehensive studies were first conducted to assess MIOCT image quality in healthy volunteers in a nonoperative setting and MIOCT visualization of instruments and maneuvers during ex vivo porcine eye surgery.[88–90] This work was fundamental to facilitate the translation of MIOCT into the human operating suite and to ensure that integration of OCT into the microscope did not negatively impact the surgeon's view. Binder et al.[85] first demonstrated intraoperative MIOCT human imaging in between surgical steps and before/after surgery using a Cirrus HD-OCT (Carl Zeiss Meditec, Oberkochen, Germany) adapted to the surgical microscope. Advantages of MIOCT outlined in that report included its ability to evaluate the completeness of ERM/ILM peeling, macular anatomy immediately after peeling, and the presence or absence of subretinal fluid. A subsequent study by Hahn et al.[91] compared intraoperative MIOCT and HHOCT imaging and confirmed that the two systems achieved comparable image quality and feedback to the surgeon during surgical pauses. Although a learning curve was noted, MIOCT maintained the advantages of HHOCT but without the need to displace the microscope away from the patient.

Intraoperative MIOCT rapidly progressed to imaging of live surgery and evaluation of instrument–retina interactions, as demonstrated in three studies published in quick succession[92–94] (Fig. 2). Falkner-Radler et al.[93] investigated the ability of MIOCT to guide ERM/ILM peeling in 70 surgical cases. Imaging was performed before, during, and after membrane peeling, and the surgeon analyzed B-scans and SVPs displayed on a monitor adjacent to the operating microscope. The authors reported that MIOCT facilitated peeling without membrane staining, and that the structural alterations due to ERM/ILM peeling detected by MIOCT—such as photoreceptor disruption and enlargement of the macular hole base—were similar to those detected in HHOCT studies previously discussed.[77] In a separate study, Hahn et al.[94] incorporated a tracking device that allowed the OCT operator to manually track the moving instrument and keep the scan centered on the region of interest. Manual tracking facilitated MIOCT imaging of surgical maneuvers such as retinal scraping during ERM removal (Fig. 2C).

Recently published studies[95–97] evaluated the performance of the RESCAN 700 (Carl Zeiss Meditec), a commercially available MIOCT system that incorporates SD-OCT technology and a monocular microscope-integrated HUD for real-time feedback to the surgeon (Figs. 3A, 3B). In the DISCOVER study,[95] the authors performed MIOCT imaging in 136 eyes undergoing posterior segment surgery for ERM, macular hole, retinal detachment, proliferative diabetic retinopathy, panuveitis, and traction retinal detachment. Key results included the demonstration of iOCT impact on surgical decision making in 19% of ERM/ILM peeling cases. In such instances, MIOCT feedback was discordant with the surgeon's impression of the completeness of peel and revealed occult membrane or lack of residual membrane. Additionally, MIOCT provided feedback that impacted surgical decision making in 21% of retinal detachment cases, such as the identification of a macular hole under perfluorocarbon liquid.[98] In another MIOCT study, Pfau et al.[96] demonstrated similar results with the RESCAN 700 in 40 surgeries. Such results included improved visual feedback of MIOCT compared to the operating microscope in 74.1% of cases, and MIOCT altering surgical decision making in 41.9% of cases. The component of MIOCT feedback that appeared to have the most impact on surgical decision making in this study was identification of ILM/ERM cleavage sites.

Translational Difficulties and Limitations

The introduction of MIOCT transformed the paradigm of live vitreoretinal surgical visualization by extending the en face view through operating microscope to high-resolution OCT tomograms. With the integration of HUD technology into MIOCT, surgeons were offered an alternative imaging modality to guide their surgeries for the first time since the 1960s. Although its advantages were demonstrated in the studies discussed above, MIOCT is still a nascent technology with important limitations.

Microscope-integrated OCT imaging of live surgery introduces confounding factors that are not present in iOCT imaging during pauses in surgery. Namely, intraocular instruments present during live surgery often cast "shadows" on underlying tissue in the B-scans. This shadowing effect was characterized during ex vivo porcine eye surgeries[88] and found to vary with instrument material, thickness, and orientation relative to the OCT optical axis. Unfortunately, instrument shadowing may preclude OCT visualization of vital instrument–retina areas of contact. Solutions to mitigate these effects include the spatial compounding of B-scans to enhance tissue visualization underneath instruments,[99] and custom instrument development to optimize OCT visibility.[100] Regarding real-time feedback, several authors noted the need to optimize the location, size, and type of OCT images displayed in the surgical oculars via the HUD.[95,96] The surgical oculars constrain the surgeon's visual field and limit the size of OCT images displayed with the HUD. Presenting OCT images on an external monitor instead could be advantageous in select scenarios due to their superior resolution and contrast compared to HUD displays.

A signification limitation of the previously described MIOCT systems is the inability to image continuous and complete instrument motion. Intraoperative real-time visualization was limited to B-scans; therefore, the maneuver of interest must be coaligned with the B-scan axis for comprehensive imaging. Since restricting surgical motion to the B-scan imaging axis is unfeasible, several authors noted the need for OCT instrument tracking. Potential solutions proposed include a manual tracking device to allow the OCT operator to target the scan location in real time,[94] and automatic instrument tracking using a stereo camera pair—albeit the latter approach is currently limited to anterior segment surgery.[101] Additionally, Hahn et al.[94] and Falkner-Radler et al.[93] discussed the potential advantages of real-time volumetric OCT acquisition to facilitate imaging of live surgery, although both noted that this approach

Investigative Ophthalmology & Visual Science

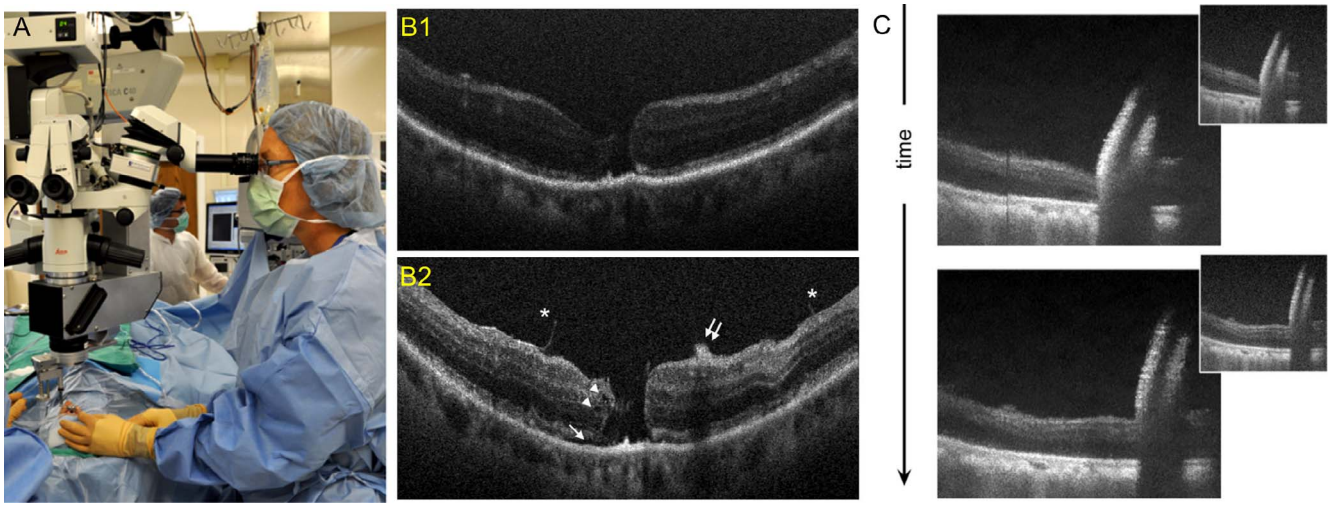

Figure 2. Live 2D microscope-integrated OCT (MIOCT) imaging of human retinal surgery. (**A**) System in use during human retinal surgery. MIOCT allows concurrent visualization of surgery with the operating microscope and OCT. (**B**) Imaging in a human patient undergoing surgery for macular hole repair. The preincision image (**B1**) depicts the macular hole and confirms the preoperative diagnosis. Imaging following internal limiting membrane peeling (ILM) (**B2**) suggests a more relaxed retinal contour, shows the location of residual ILM (*asterisks*), and reveals intraretinal hemorrhage (*double arrow*), small intraretinal cystoid spaces (*arrowheads*), and subretinal fluid (*arrow*). (**C**) Excerpts of a real-time B-scan recording of retinal brushing with a diamond-dusted retinal scraper during epiretinal membrane removal. The large images were denoised in postprocessing; the smaller *insets* are the corresponding non-postprocessed images viewable intraoperatively. (**A**, **B**) Reprinted with permission from Hahn P, Migacz J, O'Donnell R, et al. Preclinical evaluation and intraoperative human retinal imaging with a high-resolution microscope-integrated spectral domain optical coherence tomography device. *Retina*. 2013;33:1328–1337. © 2013 by Ophthalmic Communications Society, Inc.[91]; (**C**) reprinted with permission from Hahn P, Carrasco-Zevallos O, Cunefare D, et al. Intrasurgical human retinal imaging with manual instrument tracking using a microscope-integrated spectral-domain optical coherence tomography device. *Trans Vis Sci Tech*. 2015;4:1–9. © 2015 The Association for Research in Vision and Ophthalmology, Inc.[94]

was unfeasible with SD-MIOCT systems discussed thus far. In both studies, intraoperative volumetric acquisition was possible (Fig. 3), but volume rendering and visualization required intensive postprocessing.

Live Three-Dimensional OCT Imaging of Surgery

Technological Development

Real-time intraoperative imaging with all previously discussed MIOCT devices was limited to live B-scans due to the relatively slow A-scan rates of the SD-OCT systems they were based upon. Real-time volumetric MIOCT imaging could achieve more efficient assessment of live surgery and allow guidance of maneuvers with four-dimensional (4D) (volumes through time) visual feedback to the surgeon. Volumetric iOCT imaging of live model eye surgery was first demonstrated by Carrasco-Zevallos et al. in 2014 at Duke University (*IOVS* 2014;55:ARVO E-Abstract 1633). The authors constructed a custom ultrafast SS-OCT system that operated at 100-kHz A-scan rate, which was three to five times faster than previous MIOCT implementations. Custom graphic processing unit (GPU) software was also developed to acquire, process, and render volumes in real time.[102] The MIOCT mechanical interface reported by Tao et al.[81] was used to integrate the research OCT system into a commercial operating microscope (Leica Microsystems, Inc., Buffalo Grove, IL, USA). Additionally, the authors constructed a custom microscope-integrated HUD for stereoscopic visualization of iOCT volumes through the microscope oculars.[103] The integrated system (SS-MIOCT and stereoscopic HUD) was termed 4D MIOCT.

Imaging of human retinal surgery with 4D MIOCT was demonstrated in 2015 (Carrasco-Zevallos OM, et al. *IOVS* 2015;56:ARVO E-Abstract 4085). In this study, the overall volumetric frame rate depended on A-scan sampling density and varied between 3.3 and 10 volumes per second. Each OCT volume was saved immediately after acquisition in "stream saving" mode that enabled continuous volumetric recording of surgery. A dedicated operator controlled the MIOCT data acquisition parameters during surgery and was able to target the OCT scan using a manual tracking system similar to that developed by Hahn et al.[94] Volumetric data were displayed in three formats during surgery: B-scans, SVPs, and stereo volumetric renderings. The surgeon visualized the stereoscopic OCT volumes via the HUD and controlled the volume-rendering perspective with a foot-operated joystick.

Surgical Applications

The image quality of 4D MIOCT was shown to be comparable to that of intraoperative HHOCT during surgical pauses in six eyes undergoing macular hole surgery (Seider MI, et al. *IOVS* 2015;56:ARVO E-Abstract 4084). Four-dimensional MIOCT provided feedback similar to that of HHOCT to assess completeness of ERM/ILM peeling and ERM/ILM cleavage points. Additionally, 4D MIOCT provided substantially enhanced visualization of volumetric tissue deformation, which facilitated recognition of changes in 3D macular structures after surgical intervention compared to the HHOCT.

Four-dimensional MIOCT imaging of live retinal surgery has been performed in vitreoretinal cases for macular hole, ERM, myopic foveal schisis, diabetic macular edema, or retinal detachment[104] (Fig. 4) in over 100 cases to date. A substantial advantage of 4D MIOCT over previous MIOCT systems was its ability to image and record the progression of surgical maneuvers with volumetric imaging, including retinal scraping during peel initiation and membrane peeling with intraocular forceps (Figs. 4, 5). The 4D MIOCT volumes and B-scans were relayed to the surgeon via the stereoscopic HUD and provided enhanced context that augmented information obtained from

Investigative Ophthalmology & Visual Science

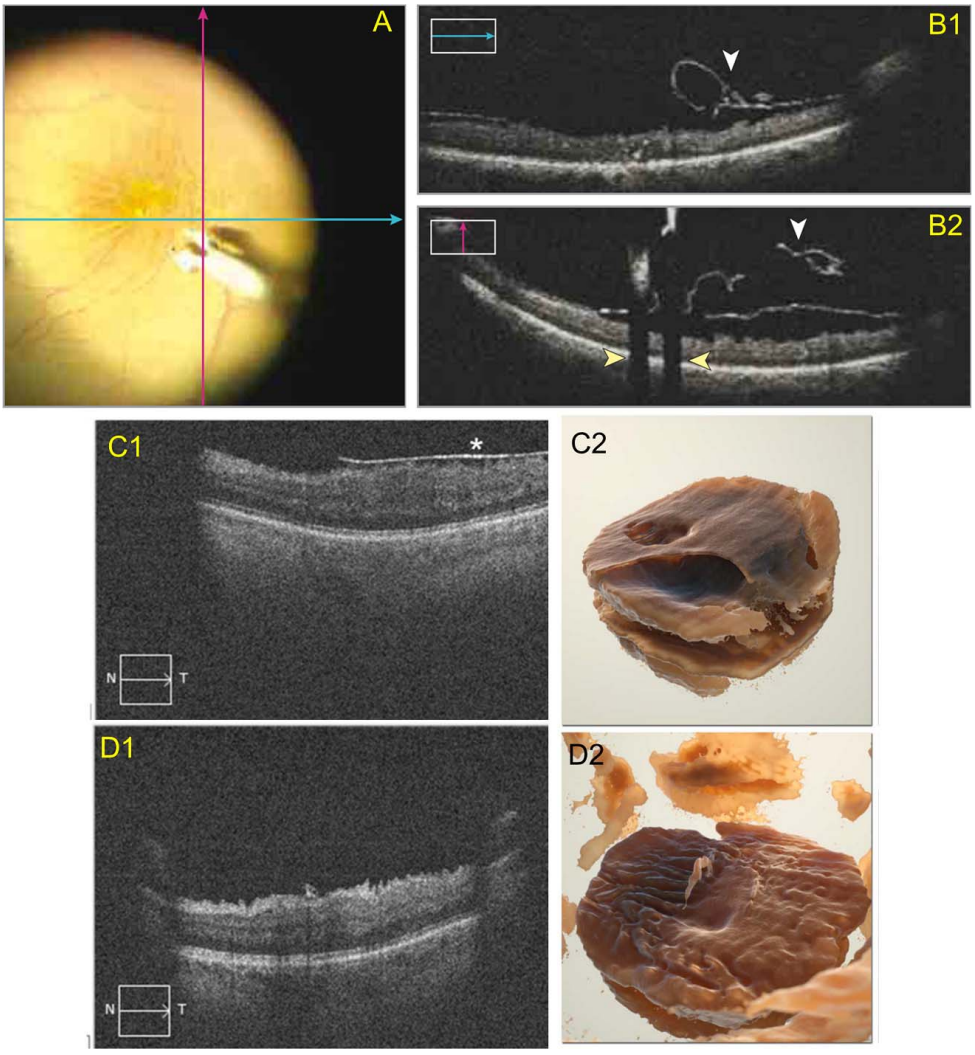

Figure 3. Live 2D MIOCT imaging of human retinal surgery with the commercially available RESCAN 700 and a Cirrus HD-OCT system adapted to an operating microscope. (**A**) Frame captured with the camera that records the surgeon's view through the operating microscope. The orthogonal *arrows* correspond to the B-scan locations. (**B**) Horizontal (**B1**) and vertical (**B2**) B-scans acquired with the RESCAN 700 during inner limiting membrane (ILM) peeling. The membrane edge (*white arrowheads*) is clearly visible in the B-scans along with "shadowing" (*yellow arrowheads*) from the intraocular forceps. (**C**) B-scan (**C1**) and volume (**C2**) acquired intraoperatively before epiretinal membrane (ERM) peeling with the reconfigured Cirrus HD-OCT system. (**D**) B-scan (**D1**) and volume (**D2**) acquired after ERM peeling. The volumes required intensive postprocessing to render and were visualized postoperatively. The prepeeling volumes depict ERM and puckering of the retina, while the postpeeling volumes show a small residual part of ERM. (**A**, **B**) Reprinted with permission from Ehlers JP, Goshe J, Dupps WJ, et al. Determination of feasibility and utility of microscope-integrated optical coherence tomography during ophthalmic surgery: the DISCOVER Study RESCAN Results. *JAMA Ophthalmol*. 2015;133:1124–1132. © 2015 American Medical Association. All rights reserved.[95]; (**C**, **D**) reprinted with permission from Falkner-Radler CI, Glittenberg C, Gabriel M, Binder S. Intrasurgical microscope-integrated spectral domain optical coherence tomography-assisted membrane peeling. *Retina*. 2015;35:2100–2106. © 2015 by Ophthalmic Communications Society, Inc.[93]

B-scan imaging alone. Key results have included enhanced visualization (compared to that with the operating microscope) of membrane elevation relative to the retinal surface over time, precise determination of instrument distance from retinal surface, and detailed visualization of retinal contour deformation during and following instrument contact (Fig. 5).[104] Moreover, the ability to control the volume-rendering orientation allowed the surgeon to inspect maneuvers from different visual perspectives (Supplementary Movie S2).

Translational Difficulties and Limitations

The extension of MIOCT to real-time volumetric imaging during live surgery overcame many of the limitations that confounded previous MIOCT implementations. Namely, live 4D visualization relaxed the constraint for constant tracking of the OCT scan to moving targets of interest. Using the stereo HUD for real-time intraoperative visualization, the surgeon could use the 4D data available to assess the surgical field and guide maneuvers in a more efficient manner compared to B-scan visualization only. However, high-quality 4D MIOCT B-scans could also be displayed via the HUD and were particularly useful for analyzing subtle structures such as ILM.

The primary limitation of this technology may be its inability to achieve volumetric frame rates that surpass the human flicker fusion rate (16 Hz). In its current iteration, even 4D MIOCT at 10 volumes per second requires sparsely distributed A-scans that result in suboptimal lateral resolution of the displayed volumes. However, recently commercialized OCT laser sources that operate at hundreds of kHz and MHz A-

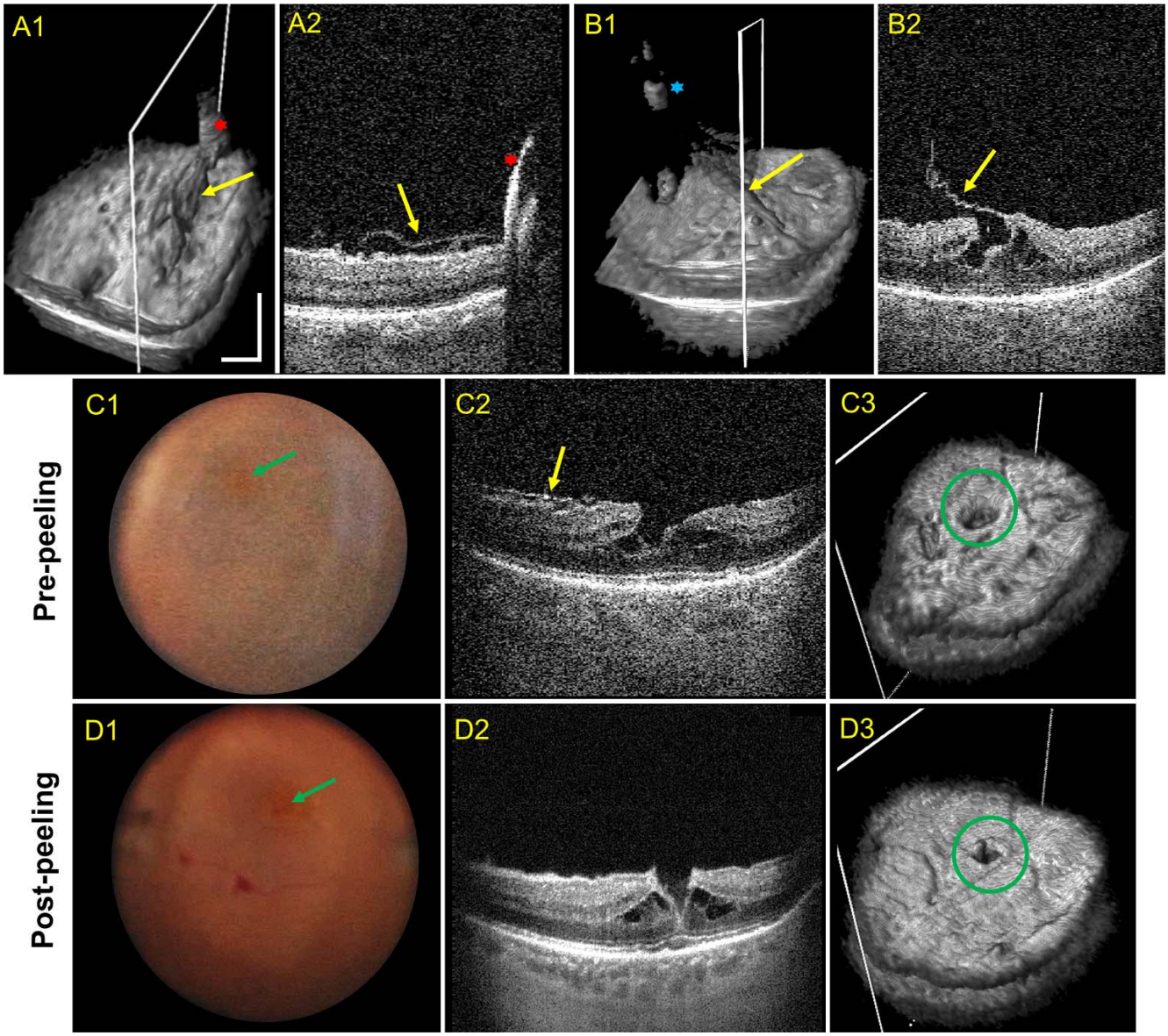

Figure 4. 4D MIOCT imaging during live human retinal surgery to remove an epiretinal membrane associated with a partial-thickness lamellar hole. All volumes and B-scans were viewable intraoperatively by the surgeon with the stereo heads-up display. (**A**) Volume (**A1**) and corresponding B-scan (**A2**) of retinal brushing with a membrane scraper (*red asterisk*) during inner limiting membrane (ILM) peeling (*yellow arrow*) (see Supplementary Movie S1). (**B**) Volume (**B1**) and corresponding B-scan (**B2**) of ILM peeling with intraocular forceps (*blue asterisk*) (see Supplementary Movie S2). The *white rectangle* on the volumes denotes the B-scan location. Instrument–ILM interaction, deformation of the lamellar hole, and underlying intraretinal cystoid spaces are shown in the images. (**C**) Prepeeling surgical visualization with a frame from the surgical camera recording (**C1**), B-scan (**C2**), and volume (**C3**). (**D**) Postpeeling visualization of the same region. Compared to the prepeeling volume, the postpeeling volume shows decreased lamellar hole size (*green*) while the B-scan confirms removal of ILM adjacent to the hole. Note the enhanced visualization of choroid (compared to SD-MIOCT at ~850 nm) due to the use of longer wavelengths for 4D MIOCT imaging. *Scale bars*: 1 mm.

scan rates could be readily implemented to overcome this limitation in the near future. Additionally, instrument shadowing first encountered in SD-MIOCT applications still presents a substantial limitation for 4D MIOCT. Volumetric imaging provides the surgeon with more context than B-scans and could facilitate surgical interpretation of the shadowed regions, but previously proposed solutions for instrument shadowing in 2D MIOCT could be applied for 4D MIOCT as well.[99,100] Finally, OCT data visualization via the stereo HUD presents limitations similar to those of the monocular HUDs in live 2D MIOCT. Specifically, concurrent OCT and microscope viewing through the oculars limits the size and resolution of the OCT images.

Discussion and Future Directions

The ongoing development and commercialization of HHOCT probes and more recently MIOCT devices may be pivotal toward the widespread clinical adoption of iOCT. This section compares currently available research-grade and commercial iOCT technology, discusses current iOCT limitations, and addresses how ongoing and future OCT technological innovations may help overcome some of these challenges.

To our knowledge, two commercial HHOCT systems have been employed in human retinal surgery to date, the Bioptigen Envisu and the Optovue iVue (Fremont, CA, USA). The Bioptigen probe is compact and lightweight and can be

Investigative Ophthalmology & Visual Science

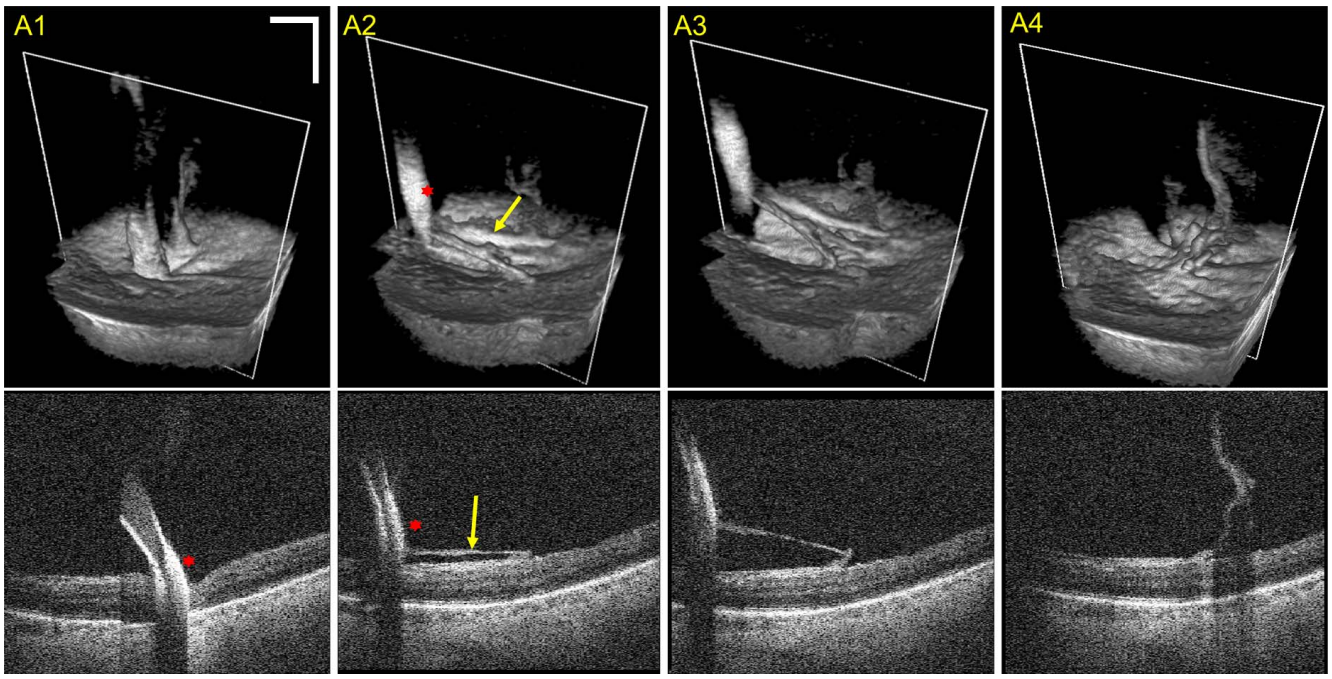

FIGURE 5. 4D MIOCT volumetric recording of retinal brushing with a membrane scraper during human retinal surgery for removal of epiretinal membrane (ERM). The images were viewable intraoperatively by the surgeon with the stereo heads-up display. Excerpts from the time series (**A1**–**A4**) are shown in volumes (*top row*) and corresponding B-scans (*bottom row*). The *white rectangle* on the volumes denotes the B-scan location. Both the membrane scraper (*red asterisk*) and ERM (*yellow arrow*) are clearly visualized in the volumes and B-scans. The volumes show retinal contour deformation during instrument contact and three-dimensional ERM structural alterations during and after brushing. Increased retinal surface tension is particularly prominent in (**A2**) and (**A3**). *Scale bars*: 1 mm.

operated in handheld mode by the surgeon[70] or mounted onto the operating microscope for added stability.[75] The Optovue iVue is heavier and typically mounted onto a stabilizing arm for intraoperative use.[67,69] Both probes must be sterilely draped to avoid contamination of the surgical field and require an OCT operator to acquire images. Both HHOCT systems also display the acquired images on external monitors for intraoperative visualization. Other important system specifications of these two HHOCT probes are included in Table 1.

Table 2 lists all commercial and research-grade MIOCT devices that have been employed in human retinal surgery to date (to the best of our knowledge). All commercial MIOCT systems utilize SD-OCT technology and are restricted to A-scan rates between 10 and 68 kHz, while the Duke SS 4D MIOCT system operated at 100 kHz. However, recent interest in high-speed OCT resulted in SD-OCT and SS-OCT prototype systems that operated at >100 kHz[107–109] and at >1 MHz[16,110,111] A-scan rates, respectively. In their current iterations, these research prototypes were not suitable for use in large-scale clinical trials, but ongoing commercialization of SS laser technology and ultrafast line scan cameras for SD may accelerate the introduction of faster OCT systems in the operating suite. Additionally, MIOCT systems operating at ~850 nm have superior resolution compared to the Duke 4D MIOCT system that operated at 1040 nm. Optical coherence tomography imaging at ~1040 nm, however, is not degraded by indocyanine green dye (absorption maximum at ~800 nm) staining of tissue, and achieves enhanced imaging of the choroid[112] and improved visibility through cataracts[113] and corneal edema.[114] This enhanced visibility can be valuable in complex and lengthy ocular surgeries.

Real-time MIOCT visualization of live surgery requires HUD technology to relay the images directly into the surgeon's oculars, and optimizing OCT feedback without altering the surgeon's view through the operating microscope can be challenging. Current MIOCT HUDs use microdisplays to project the OCT images into a small portion of the surgeon's visual field through the oculars to avoid obstructing the surgery view. Microdisplays are compact and can help reduce the footprint of the HUD to facilitate their integration into the microscope. However, the limited resolution of current microdisplays may restrict the size and resolution of the displayed OCT images, and multiple microdisplays could be required for a binocular HUD. Alternatively, the Duke MIOCT HUD employed a spatial multiplexing scheme to achieve a binocular stereo presentation of OCT volumes with only one microdisplay.[103] The Zeiss RESCAN 700 also uses the HUD to display cross-hairs over the fundus view to denote the OCT scan location to the surgeon.

Most MIOCT systems also allow the surgeon to control aspects of the OCT acquisition and/or visualization in real time. The Zeiss RESCAN 700 allows the surgeon to control the lateral OCT scan location with a foot pedal,[95] while the Haag-Streit Surgical system allows the surgeon to turn the OCT display on and off with a foot-activated switch.[83] In the Duke 4D MIOCT system, the foot pedal allowed the surgeon to alter the rendering perspective of the stereo volumes displayed via the HUD.[104] Control of the surgical viewpoint empowers the surgeon to examine tissue beneath and around a complex surgical site, for example, the surgeon can examine a retinal break from a viewpoint beneath an elevated membrane. Visualization of the retinal surface from alternative viewpoints has been previously demonstrated with an intraocular monocular endoscope[115]; however, the endoscopic approach was limited to surface imaging only and would require excision of tissue for submembrane viewing, rendering this technique unfeasible for intraretinal viewing. In contrast, 4D MIOCT volumetric visualization allows the surgeon to inspect both epi- and intraretinal structures noninvasively from arbitrary perspectives.

Investigative Ophthalmology & Visual Science

Table 1. System Specifications and Features of Commercial HHOCT Systems Used in Human Retinal Surgery to Date*

System	OCT Technology	Speed, Resolution, Wavelength	Primary Visualization Modes	Modes of Operation	Commercial Status
Bioptigen Envisu[70,76,105]	Spectral domain	17k–32k†, 3–5† μm, 870 nm	B-scans, en face on external monitor	Handheld, mounted onto microscope	FDA approved
Optovue iVue[69,106]	Spectral domain	26K, 5 μm, 840 nm	B-scans, volumes, en face on external monitor	Mounted onto stabilizing arm	FDA approved

* Speed is listed in terms of A-scans/second; resolution refers to axial resolution; wavelength refers to the central wavelength of the source.
† Not specified in publications. Range provided by manufacturer.

All MIOCT systems, except the Zeiss RESCAN 700, utilize a modular MIOCT scanner that is not permanently attached to the operating microscope. The modular design allows the MIOCT scanner to be used with multiple microscopes and facilitates MIOCT imaging in multiple operating suites with one system. The MIOCT attachment point on the microscope varies between systems; most MIOCT scanners are attached prior to the microscope objective and after the zoom optics, while the Haag-Streit iOCT is mounted onto the camera port of the microscope and the OCT beam is projected through the microscope zoom optics. As a result, the lateral resolution of the Haag-Streit iOCT system can be controlled using the microscope's optical zoom,[83] while the lateral resolution of the other modular MIOCT scanners is independent of the

Table 2. System Specifications and Features of All Research-Grade and Commercial MIOCT Systems Used in Human Retinal Surgery to Date*

System	OCT Technology	Speed, Resolution, Wavelength	Primary Visualization Modes	OCT Acquisition and Features	OCT Scanner Design	Commercial Status
Live 2D MIOCT						
Duke 2010,[81] Bioptigen Envisu engine	Spectral domain	20k, 5 μm, 840 nm	Live B-scans, static en face on external monitor	OCT operator control with manual tracking	Modular	Research prototype
Vienna 2011,[85,93,116] Zeiss Cirrus HD-OCT engine	Spectral domain	27k–68k†, 5 μm, 840 nm	Live B-scans, static en face on external monitor	OCT operator control	Modular	Research prototype
Cleveland Clinic 2015,[84] Bioptigen Envisu engine	Spectral domain	36k, 5.2 μm, 870 nm	Live B-scans on monocular, monoscopic HUD	OCT operator control with tunable focus lens	Modular	Research prototype
Zeiss RESCAN 700[96,98,117]	Spectral domain	27k, 5.5 μm, 840 nm	Live B-scans on monocular, monoscopic HUD	OCT operator control with z-tracking, surgeon control of OCT scan location via foot pedal	Permanently integrated	FDA approved
Haag-Streit Surgical iOCT[83,118,119]	Spectral domain	10k, 10 μm, 840 nm	Live B-scans on binocular, monoscopic HUD	OCT operator control, surgeon control of OCT display via foot pedal, optical zoom	Modular	FDA approved
Bioptigen EnFocus[120]	Spectral domain	32k, 4 μm, 860 nm	Live B-scans, static en face on external monitor	OCT operator control, surgeon control via foot pedal	Modular	FDA approved
Live 3D MIOCT						
Duke 2015[104]	Swept source	100k, 7.8 μm, 1040 nm	Live B-scan and live stereo volumes on binocular stereo HUD	OCT operator control with manual tracking, surgeon control of volume-rendering perspective via foot pedal	Modular	Research prototype

* Speed is listed in terms of A-scans/second; resolution refers to axial resolution; wavelength refers to the central wavelength of the source.
† Not specified in publications. Range provided by manufacturer.

Investigative Ophthalmology & Visual Science

microscope's optical zoom. In contrast to the modular design, the Zeiss RESCAN 700 employs a fully integrated design in which the MIOCT scanner is permanently attached to the operating microscope. The primary benefit of this approach is that the mechanical and optical integration of the two modalities can be optimized such that the overall footprint and physical appearance of the microscope is minimally altered.[95]

Imaging of live surgery with MIOCT presents unique challenges compared to imaging at surgical pauses with handheld probes. In particular, the introduction of intraocular instruments causes shadowing that may result in suboptimal visualization of underlying retinal tissue. Smaller-gauge instruments were found to shadow less in general, but shadowing also varied due to instrument material, design, and orientation relative to the OCT imaging axis.[88] Optical coherence tomography–compatible instrument prototypes composed of semitransparent material in the near-infrared have been demonstrated[100] and allowed OCT visualization with significantly reduced shadowing, but the surgical functionality of these instruments has yet to be rigorously evaluated. The recent commercialization of MIOCT devices, however, may catalyze the further development and commercialization of such instruments as MIOCT systems become more commonplace in operating suites worldwide. A second factor that may degrade MIOCT live surgical imaging is eye motion due to the voluntary patient motion and/or surgical maneuvers. In both cases, retinal tracking may be desired to generate iOCT images with minimal motion artifacts. The Zeiss RESCAN 700 MIOCT utilizes "z-tracking" to automatically adjust the reference arm delay to compensate for axial motion. This technique may be particularly useful in surgical cases involving large axial motion, such as retinal detachment repairs. Previously demonstrated implementations of real-time retinal tracking[32,121,122] to compensate for lateral motion require additional hardware that could increase the size of the MIOCT scanners, but the benefits of motion-compensated iOCT, especially during volumetric imaging, may justify these hardware additions. Furthermore, automated surgical instrument tracking could also help center the iOCT scans on the region of interest in the presence of motion. Several previous instrument tracking implementations used a fundus camera[123,124] for tracking, and another implementation employed a stereo camera pair to localize and track the instrument.[101] However, the former technique has not been integrated with iOCT, and the latter is currently limited to iOCT imaging in anterior eye surgery.

Qualitative visual assessment of the surgical field is the primary intraoperative feedback mechanism allowed by current iOCT technology. Retinal OCT image-processing techniques, such as retinal layer segmentation,[29] are now commonplace and can provide to the clinician quantitative metrics to assess pathology. Such algorithms have been applied to iOCT data postoperatively to analyze anatomical alterations that occurred during surgical repair,[72,77] but their intraoperative application could provide quantitative feedback to surgeons about the impact of their maneuvers in real time. Additional surgery-specific algorithms, such as real-time calculation of the retina–instrument distance based on OCT data, could help increase the precision and repeatability of maneuvers by providing quantitative metrics. Secondary forms of feedback to the surgeon, such as auditory signals indicating the instrument distance to the retinal surface, could also be facilitated by these quantitative metrics.

Due to its versatility and historical importance, the operating microscope is an irreplaceable instrument for current retinal surgery. Yet iOCT systems can provide unique feedback regarding the retinal anatomy and retina–instrument interactions, which in select scenarios results in superior visualization compared to the operating microscope. Therefore, it is not unreasonable to posit that MIOCT image guidance as the primary (or only) mode of visualization may be desirable in select surgical scenarios, although significant testing and development would be required before such alternate visualization modes are used routinely in human surgery. The feasibility of 4D MIOCT imaged-guided retinal surgery without the operating microscope view has been evaluated in an ex vivo pilot study by Toth et al. (*IOVS* 2015;56:ARVO E-Abstract 3512). Surgical maneuvers in porcine eyes were initially performed with the operating microscope view augmented by 4D MIOCT (as performed during human surgery imaging). The surgeons then operated under 4D MIOCT guidance alone (without the fiberoptic illumination) using either the stereoscopic HUD or an external 3D monitor with viewing eyewear (Nvidia Corporation, Santa Clara, CA, USA). The surgeons performed simulated membrane peeling, retinal surface scraping, and intra- and subretinal placement of instruments and delivery of subretinal materials. Four-dimensional MIOCT provided sufficient orientation, context, and structural detail of the retinal surface to perform accurate and smooth maneuvers, albeit at a slow pace due to the limited volumetric frame rate. Unique advantages of exclusive 4D MIOCT guidance included the ability to perform bimanual maneuvers without the need for intraocular visible light illumination, and the ability to reorient the volume to view intra- and subretinal structures and instruments during surgical manipulation.

Conclusions

Retinal surgery visualization with the operating microscope, while revolutionary when first introduced, currently limits the surgeon's depth perception and assessment of subtle microanatomy. The development of retinal iOCT has dramatically enhanced intraoperative feedback to the surgeon. As iOCT applications evolve from imaging during surgical pauses to 4D image-guided surgery, the improved visualization afforded by these systems may lead to refinement of surgical techniques and development of novel procedures enabled by real-time tomographic and volumetric visualization.

Acknowledgments

Supported by National Institutes of Health (NIH)/National Eye Institute Biomedical Research Partnership Grant R01-EY023039 "Intraoperative OCT Guidance of Intraocular Surgery" and a National Science Foundation Graduate Research Fellowship, Ford Foundation Predoctoral Fellowship, and NIH T-32 Training Grant awarded to OMC-Z.

The intraoperative OCT systems at Duke University are nonsignificant risk investigational devices as defined in Food and Drug Administration (FDA) guidelines 21 CFR 812. These devices are used in minimal risk studies under a Duke University Health System (DUHS) Institutional Review Board (IRB)-approved research protocol, Pro00016827.

Disclosure: **O.M. Carrasco-Zevallos**, None; **B. Keller**, None; **C. Viehland**, None; **L. Shen**, None; **M.I. Seider**, None; **J.A. Izatt**, Leica Microsystems (R), P, Bioptigen (I, R, S), P; **C.A. Toth**, Genetech (F), Bioptigen (F), Alcon (R), ThromboGenics (C)

References

1. Daniel RK. Microsurgery: through the looking glass. *N Engl J Med*. 1979;300:1251–1257.

2. Barraquer J, Barraquer J, Littman HA. New operating microscope for ocular surgery. *Am J Ophthalmol*. 1967;63: 90–97.
3. Harms H, Mackensen G. *Ocular Surgery Under the Microscope*. Chicago: Year Book Medical Publishers; 1967.
4. Machemer R, Buettner H, Norton E, Parel J. Vitrectomy: a pars plana approach. *Trans Am Acad Ophthalmol*. 1971;75:813–820.
5. Machemer R. The development of pars plana vitrectomy: a personal account. *Graefes Arch Clin Exp Ophthalmol*. 1995; 233:453–468.
6. Machemer R. A new concept for vitreous surgery. 7. Two instrument techniques in pars plana vitrectomy. *Arch Ophthalmol*. 1974;92:407.
7. Parel J, Machemer R, Aumayr W. A new concept for vitreous surgery. 4. Improvements in instrumentation and illumination. *Am J Ophthalmol*. 1974;77:6–12.
8. Parel JM, Machemer R, Aumayr W. A new concept for vitreous surgery. 5. An automated operating microscope. *Am J Ophthalmol*. 1974;77:161–168.
9. Fabian ID, Moisseiev J. Sutureless vitrectomy: evolution and current practices. *Br J Ophthalmol*. 2011;95:318–324.
10. Eckardt C. Twin lights: a new chandelier illumination for bimanual surgery. *Retina*. 2003;23:893–894.
11. Spitznas M. A binocular indirect ophthalmomicroscope (BIOM) for non-contact wide-angle vitreous surgery. *Graefes Arch Clin Exp Ophthalmol*. 1987;225:13–15.
12. Huang D, Swanson EA, Lin CP, et al. Optical coherence tomography. *Science*. 1991;254:1178–1181.
13. Rollins A, Yazdanfar S, Kulkarni M, Ung-Arunyawee R, Izatt J. In vivo video rate optical coherence tomography. *Opt Express*. 1998;3:219–229.
14. Nassif NA, Cense B, Park BH, et al. In vivo high-resolution video-rate spectral-domain optical coherence tomography of the human retina and optic nerve. *Opt Express*. 2004;12:367–376.
15. Choi D-H, Hiro-Oka H, Shimizu K, Ohbayashi K. Spectral domain optical coherence tomography of multi-MHz A-scan rates at 1310 nm range and real-time 4D-display up to 41 volumes/second. *Biomed Opt Express*. 2012;3:3067–3086.
16. Wieser W, Draxinger W, Klein T, Karpf S, Pfeiffer T, Huber R. High definition live 3D-OCT in vivo: design and evaluation of a 4D OCT engine with 1 GVoxel/s. *Biomed Opt Express*. 2014;5:2963.
17. Choma M, Sarunic M, Yang C, Izatt J. Sensitivity advantage of swept source and Fourier domain optical coherence tomography. *Opt Express*. 2003;11:2183–2189.
18. Toth CA, Narayan DG, Boppart SA, et al. A comparison of retinal morphology viewed by optical coherence tomography and light microscopy. *Arch Ophthalmol*. 1997;115:1425–1428.
19. Toth CA, Birngruber R, Boppart SA, et al. Argon laser retinal lesions evaluated in vivo by optical coherence tomography. *Am J Ophthalmol*. 1997;123:188–198.
20. Swanson EA, Izatt JA, Hee MR, et al. In vivo retinal imaging by optical coherence tomography. *Opt Lett*. 1993;18:1864–1866.
21. Puliafito CA, Hee MR, Lin CP, et al. Imaging of macular diseases with optical coherence tomography. *Ophthalmology*. 1995;102:217–229.
22. Hee MR, Puliafito CA, Wong C, et al. Optical coherence tomography of macular holes. *Am J Ophthalmol*. 1995;102: 748–756.
23. Hee MR, Puliafito CA, Wong C, et al. Quantitative assessment of macular edema with optical coherence tomography. *Arch Ophthalmol*. 1995;113:1019–1029.
24. Hee MR, Baumal CR, Puliafito CA, et al. Optical coherence tomography of age-related macular degeneration and choroidal neovascularization. *Ophthalmology*. 1996;103:1260–1270.
25. Schuman JS, Hee MR, Puliafito CA, et al. Quantification of nerve fiber layer thickness in normal and glaucomatous eyes using optical coherence tomography. *Arch Ophthalmol*. 1995;113:586–596.
26. Tan O, Chopra V, Lu ATH, et al. Detection of macular ganglion cell loss in glaucoma by Fourier-domain optical coherence tomography. *Ophthalmology*. 2009;116:2305–2314, e2.
27. Cabrera Fernández D, Salinas HM, Puliafito CA. Automated detection of retinal layer structures on optical coherence tomography images. *Opt Express*. 2005;13:10200.
28. Ishikawa H, Stein DM, Wollstein G, Beaton S, Fujimoto JG, Schuman JS. Macular segmentation with optical coherence tomography. *Invest Ophthalmol Vis Sci*. 2005;46:2012–2017.
29. Chiu SJ, Li XT, Nicholas P, Toth CA, Izatt JA, Farsiu S. Automatic segmentation of seven retinal layers in SDOCT images congruent with expert manual segmentation. *Opt Express*. 2010;18:19413–19428.
30. Kolb JP, Klein T, Kufner CL, Wieser W, Neubauer AS, Huber R. Ultra-widefield retinal MHz-OCT imaging with up to 100 degrees viewing angle. *Biomed Opt Express*. 2015;6:1534–1552.
31. McNabb RP, Grewal DS, Mehta R, et al. Wide field of view of swept-source optical coherence tomography for peripheral retinal disease [published online ahead of print January 11, 2016]. *Br J Ophthalmol*. doi:10.1136/bjophthalmol-2015-307480.
32. Vienola KV, Braaf B, Sheehy CK, et al. Real-time eye motion compensation for OCT imaging with tracking SLO. *Biomed Opt Express*. 2012;3:2950–2963.
33. Carrasco-Zevallos OM, Nankivil D, Keller B, Viehland C, Lujan BJ, Izatt JA. Pupil tracking optical coherence tomography for precise control of pupil entry position. *Biomed Opt Express*. 2015;6:3405–3419.
34. Yazdanfar S, Rollins AM, Izatt JA. Imaging and velocimetry of the human retinal circulation with color Doppler optical coherence tomography. *Opt Lett*. 2000;25:1448–1450.
35. Makita S, Hong Y, Yamanari M, Yatagai T, Yasuno Y. Optical coherence angiography. *Opt Express*. 2006;14:7821–7840.
36. Wang RK, Jacques SL, Ma Z, Hurst S, Hanson SR, Gruber A. Three dimensional optical angiography. *Opt Express*. 2007; 15:4083–4097.
37. Szkulmowska A, Szkulmowski M, Szlag D, Kowalczyk A, Wojtkowski M. Three-dimensional quantitative imaging of retinal and choroidal blood flow velocity using joint spectral and time domain optical coherence tomography. *Opt Express*. 2009;17:10584–10598.
38. Kim DY, Fingler J, Zawadzki RJ, et al. Optical imaging of the chorioretinal vasculature in the living human eye. *Proc Natl Acad Sci U S A*. 2013;110:14354–14359.
39. Jia Y, Bailey ST, Hwang TS, et al. Quantitative optical coherence tomography angiography of vascular abnormalities in the living human eye. *Proc Natl Acad Sci U S A*. 2015; 12:2395–2402.
40. Wilkins JR, Puliafito CA, Hee MR, et al. Characterization of epiretinal membranes using optical coherence tomography. *Ophthalmology*. 1996;103:2142–2151.
41. Ripandelli G, Coppe A, Bonini S, et al. Morphological evaluation of full-thickness idiopathic macular holes by optical coherence tomography. *Eur J Ophthalmol*. 1999;9: 212–216.
42. Mikajiri K, Okada AA, Ohji M, et al. Analysis of vitrectomy for idiopathic macular hole by optical coherence tomography. *Am J Ophthalmol*. 1999;128:655–657.

Investigative Ophthalmology & Visual Science

43. Gallemore RP, Jumper MJ, McCuen B II, Jaffe GJ, Postel EA, Toth CA. Diagnosis of vitreoretinal adhesions in macular disease with optical coherence tomography. *Retina*. 2000;20:115–120.
44. Massin P, Allouch C, Haouchine B, et al. Optical coherence tomography of idiopathic macular epiretinal membranes before and after surgery. *Am J Ophthalmol*. 2000;130:732–739.
45. Falkner-Radler CI, Glittenberg C, Hagen S, Benesch T, Binder S. Spectral-domain optical coherence tomography for monitoring epiretinal membrane surgery. *Ophthalmology*. 2010;117:798–805.
46. Jumper MJ, Gallemore RP, McCuen BW, Toth CA. Features of macular hole closure in the early portoperative period using optical coherence tomography. *Retina*. 2000;20:232–237.
47. Kasuga Y, Arai J, Akimoto M, Yoshimura N. Optical coherence tomography to confirm early closure of macular holes. *Am J Ophthalmol*. 2000;130:675–676.
48. Ip MS, Baker BJ, Duker JS, et al. Anatomical outcomes of surgery for idiopathic macular hole as determined by optical coherence tomography. *Arch Ophthalmol*. 2002;120:29–35.
49. Inoue M, Watanabe Y, Arakawa A, Sato S, Kobayashi S, Kadonosono K. Spectral-domain optical coherence tomography images of inner/outer segment junctions and macular hole surgery outcomes. *Graefes Arch Clin Exp Ophthalmol*. 2009;247:325–330.
50. Imai M, Iijima H, Gotoh T, Tsukahara S. Optical coherence tomography of macular holes. *Am J Ophthalmol*. 1999;128:621–627.
51. Massin P, Duguid G, Erginay A, Haouchine B, Gaudric A. Optical coherence tomography for evaluating diabetic macular edema before and after vitrectomy. *Am J Ophthalmol*. 2003;135:169–177.
52. Kaiser PK, Riemann CD, Searrs J, Lewis H. Vitrectomy for diabetic macular traction and edema associated with posterior hyaloidal traction. *Ophthalmology*. 2001;131:44–49.
53. Akiba J, Konno S, Sato E, Yoshida A. Retinal detachment and retinoschisis detected by optical coherence in a myopic eye with a macular hole. *Ophthalmic Surg Lasers Imaging*. 2000;31:240–242.
54. Kumagai K, Furukawa M, Ogino N, Larson E. Factors correlated with postoperative visual acuity after vitrectomy and internal limiting membrane peeling for myopic foveoschisis. *Retina*. 2010;30:874–880.
55. Scott AW, Farsiu S, Enyedi LB, Wallace DK, Toth CA. Imaging the infant retina with a hand-held spectral-domain optical coherence tomography device. *Am J Ophthalmol*. 2009;147:364–373, e2.
56. Boppart SA, Brezinski ME, Pitris C, Fujimoto JG. Optical coherence tomography for neurosurgical imaging of human intracortical melanoma. *Neurosurgery*. 1998;43:834–841.
57. Brezinski ME, Tearney GJ, Boppart SA, Swanson EA, Southern JF, Fujimoto JG. Optical biopsy with optical coherence tomography: feasibility for surgical diagnostics. *J Surg Res*. 1997;71:32–40.
58. Boppart SA, Bouma BE, Pitris C, et al. Intraoperative assessment of microsurgery with three-dimensional optical coherence tomography. *Radiology*. 1998;208:81–86.
59. Boppart SA, Herrmann JM, Pitris C, Stamper DL, Brezinski ME, Fujimoto JG. Real-time optical coherence tomography for minimally invasive imaging of prostate ablation. *Comput Aided Surg*. 2001;6:94–103.
60. Shakhov AV, Terentjeva AB, Kamensky VA, et al. Optical coherence tomography monitoring for laser surgery of laryngeal carcinoma. *J Surg Oncol*. 2001;77:253–258.
61. Boppart SA, Bouma BE, Pitris C, Tearney GJ, Fujimoto JG, Brezinski ME. Forward-imaging instruments for optical coherence tomography. *Opt Lett*. 1997;22:1618–1620.
62. Radhakrishnan S, Rollins AM, Roth JE, et al. Real-time optical coherence tomography of the anterior segment at 1310 nm. *Arch Ophthalmol*. 2001;119:1179–1185.
63. Chavala SH, Farsiu S, Maldonado R, Wallace DK, Freedman SF, Toth CA. Insights into advanced retinopathy of prematurity using handheld spectral domain optical coherence tomography imaging. *Ophthalmology*. 2009;116:2448–2456.
64. Maldonado RS, O'Connell RV, Sarin N, et al. Dynamics of human foveal development after premature birth. *Ophthalmology*. 2011;118:2315–2325.
65. Maldonado RS, Izatt JA, Sarin N, et al. Optimizing hand-held spectral domain optical coherence tomography imaging for neonates, infants, and children. *Invest Ophthalmol Vis Sci*. 2010;51:2678–2685.
66. Rothman AL, Folgar FA, Tong AY, Toth CA. Spectral domain optical coherence tomography characterization of pediatric epiretinal membranes. *Retina*. 2014;34:1323–1334.
67. Pichi F, Alkabes M, Nucci P, Ciardella AP. Intraoperative SD-OCT in macular surgery. *Ophthal Surg Lasers Imaging*. 2012;43:54–60.
68. Riazi-Esfahani M, Khademi M, Mazloumi M, Khodabandeh A, Riazi-Esfahani H. Macular surgery using intraoperative spectral domain optical coherence tomography. *J Ophthalmic Vis Res*. 2015;10:309.
69. Branchini LA, Gurley K, Duker JS, Reichel E. Use of handheld intraoperative spectral-domain optical coherence tomography in a variety of vitreoretinal diseases. *Ophthalmic Surg Lasers Imaging*. 2016;47:49–55.
70. Dayani PN, Maldonado R, Farsiu S, Toth CA. Intraoperative use of handheld spectral domain optical coherence tomography imaging in macular surgery. *Retina*. 2009;29:1457–1468.
71. Wykoff CC, Berrocal AM, Schefler AC, Uhlhorn SR, Ruggeri M, Hess D. Intraoperative OCT of a full-thickness macular hole before and after internal limiting membrane peeling. *Ophthalmic Surg Lasers Imaging*. 2010;41:7–11.
72. Ehlers JP, Kernstine K, Farsiu S, Neeru S, Maldonado RS, Toth CA. Analysis of pars plana vitrectomy for optic pit–related maculopathy with intraoperative optical coherence tomography: a possible connection with the vitreous cavity. *Arch Ophthalmol*. 2011;129:1483–1486.
73. Henry CR, Berrocal AM, Hess DJ, Murray TG. Intraoperative spectral-domain optical coherence tomography in Coats' disease. *Ophthalmic Surg Lasers Imaging*. 2012;43:e80–e84.
74. Nam DH, Desouza P, Hahn P, et al. Intraoperative spectral domain optical coherence tomography imaging after internal limiting membrane peeling in idiopathic epiretinal membrane with connecting strands. *Retina*. 2015;35:1622–1630.
75. Ray R, Barañano DE, Fortun JA, et al. Intraoperative microscope-mounted spectral domain optical coherence tomography for evaluation of retinal anatomy during macular surgery. *Ophthalmology*. 2011;118:2212–2217.
76. Ehlers JP, Dupps WJ, Kaiser PK, et al. The Prospective Intraoperative and Perioperative Ophthalmic ImagiNg With Optical CoherEncE TomogRaphy (PIONEER) study: 2-year results. *Am J Ophthalmol*. 2014;158:999–1007, e1.
77. Ehlers JP, Xu D, Kaiser P, Singh R, Srivastava S. Intrasurgical dynamics of macular hole surgery: an assessment of surgery-induced ultrastructural alterations with intraoperative optical coherence tomography. *Retina*. 2014;34:213–221.
78. Ehlers JP, Tam T, Kaiser P, Martin D, Smith G, Srivastava S. Utility of intraoperative optical coherence tomography during vitrectomy surgery for vitreomacular traction syndrome. *Retina*. 2014;34:1341–1346.
79. Ehlers JP, Ohr MP, Kaiser PK, Srivastava SK. Novel microarchitectural dynamics in rhegmatogenous retinal detachments identified with intraoperative optical coherence tomography. *Retina*. 2013;33:1428–1434.

80. Ehlers JP, Han J, Petkovsek D, Kaiser PK, Singh RP, Srivastava SK. Membrane peeling-induced retinal alterations on intraoperative OCT in vitreomacular interface disorders from the PIONEER Study. *Invest Ophthalmol Vis Sci*. 2015;56:7324–7330.
81. Tao YK, Ehlers JP, Toth CA, Izatt JA. Intraoperative spectral domain optical coherence tomography for vitreoretinal surgery. *Opt Lett*. 2010;35:3315–3317.
82. Geerling G, Müller M, Winter C, et al. Intraoperative 2-dimensional optical coherence tomography as a new tool for anterior segment surgery. *Arch Ophthalmol*. 2005;123:253–257.
83. Siebelmann S, Steven P, Hos D, Lankenau E, Bachmann B, Cursiefen C. Advantages of microscope-integrated intraoperative online optical coherence tomography: usage in Boston keratoprosthesis type I surgery. *J Biomed Opt*. 2016;21:0160051–0160056.
84. Tao YK, Srivastava SK, Ehlers JP. Microscope-integrated intraoperative OCT with electrically tunable focus and heads-up display for imaging of ophthalmic surgical maneuvers. *Biomed Opt Express*. 2014;5:1877–1885.
85. Binder S, Falkner-Radler CI, Hauger C, Matz H, Glittenberg C. Feasibility of intrasurgical spectral-domain optical coherence tomography. *Retina*. 2011;31:1332–1336.
86. Migacz J, Carrasco-Zevallos OM, Hahn P, Kuo AN, Toth CA, Izatt JA. Intraoperative retinal optical coherence tomography. In: *Optical Coherence Tomography: Technology and Applications*. Switzerland: Springer International Publishing; 2015:1771–1796.
87. Hahn P, Migacz J, O'Connell R, Maldonado RS, Izatt JA, Toth CA. The use of optical coherence tomography in intraoperative ophthalmic imaging. *Ophthalmic Surg Lasers Imaging*. 2011;42:S85–S94.
88. Ehlers JP, Tao YK, Farsiu S, Maldonado R, Izatt JA, Toth CA. Integration of a spectral domain optical coherence tomography system into a surgical microscope for intraoperative imaging. *Invest Ophthalmol Vis Sci*. 2011;52:3153–3159.
89. Ehlers JP, Tao YK, Farsiu S, Maldonado R, Izatt JA, Toth CA. Visualization of real-time intraoperative maneuvers with a microscope-mounted spectral domain optical coherence tomography system. *Retina*. 2013;33:232–236.
90. Hahn P, Migacz J, O'Connell R, Izatt JA, Toth CA. Unprocessed real-time imaging of vitreoretinal surgical maneuvers using a microscope-integrated spectral-domain optical coherence tomography system. *Graefes Arch Clin Exp Ophthalmol*. 2013;251:213–220.
91. Hahn P, Migacz J, O'Connell R, et al. Preclinical evaluation and intraoperative human retinal imaging with a high-resolution microscope-integrated spectral domain optical coherence tomography device. *Retina*. 2013;33:1328–1337.
92. Ehlers JP, Kaiser PK, Srivastava SK. Intraoperative optical coherence tomography utilizing the RESCAN 700: preliminary results from the DISCOVER study. *Br J Ophthalmol*. 2014;98:1329–1332.
93. Falkner-Radler C, Glittenberg C, Gabriel M, Binder S. Intrasurgical microscope-integrated spectral domain optical coherence tomography assisted membrane peeling. *Retina*. 2015;35:2100–2106.
94. Hahn P, Carrasco-Zevallos O, Cunefare D, et al. Intrasurgical human retinal imaging with manual instrument tracking using a microscope-integrated spectral-domain optical coherence tomography device. *Trans Vis Sci Tech*. 2015;4:1–9.
95. Ehlers JP, Goshe J, Dupps WJ, et al. Determination of feasibility and utility of microscope-integrated optical coherence tomography during ophthalmic surgery. *JAMA Ophthalmol*. 2015;133:1124–1132.
96. Pfau M, Michels S, Binder S, Becker MD. Clinical experience with the first commercially available intraoperative optical coherence tomography system. *Ophthalmic Surg Lasers Imaging Retina*. 2015;46:1001–1008.
97. Jayadev C, Dabir S, Vinekar A, Shah U, Vaid T, Kumar Yadav N. Microscope-integrated optical coherence tomography: a new surgical tool in vitreoretinal surgery. *Indian J Ophthalmol*. 2015;63:399–403.
98. Smith AG, Cost BM, Ehlers JP. Intraoperative OCT-assisted subretinal perfluorocarbon liquid removal in the DISCOVER study. *Ophthalmic Surg Lasers Imaging Retina*. 2015;46:964–966.
99. Tao YK, Ehlers JP, Toth CA, Izatt JA. Visualization of vitreoretinal surgical manipulations using intraoperative spectral domain optical coherence tomography. *Proc SPIE*. 2011;7889:78890F.1–9.
100. Ehlers JP, Srivastava SK, Feiler D, Noonan AI, Rollins AM, Tao YK. Integrative advances for OCT-guided ophthalmic surgery and intraoperative OCT: microscope integration, surgical instrumentation, and heads-up display surgeon feedback. *PLoS One*. 2014;9:e105224.
101. El-Haddad MT, Tao YK. Automated stereo vision instrument tracking for intraoperative OCT guided anterior segment ophthalmic surgical maneuvers. *Biomed Opt Express*. 2015;6:3014.
102. Viehland C, Keller B, Carrasco-Zevallos OM, et al. Enhanced volumetric visualization for real time 4D intraoperative ophthalmic swept-source OCT. *Biomed Opt Express*. 2016;7:1815–1829.
103. Shen L, Carrasco-Zevallos OM, Keller B, et al. Novel microscope-integrated stereoscopic heads-up display for intrasurgical optical coherence tomography. *Biomed Opt Express*. 2016;7:1711–1726.
104. Carrasco-Zevallos OM, Keller B, Viehland C, et al. 4D microscope-integrated OCT improves accuracy of ophthalmic surgical maneuvers. *Proc SPIE*. 2016;9693:969306.1–7.
105. Leica Microsystems Envisu C-Class technical specifications. Leica Microsystems website. Available at: http://www.leica-microsystems.com/products/optical-coherence-tomography-oct/details/product/envisu-c-class/. Accessed April 18, 2016.
106. Optovue iVue technical specifications. Optovue website. Available at: http://www.optovue.com/products/ivue/. Accessed April 18, 2016.
107. Zhang K, Kang JU. Real-time intraoperative 4D full-range FD-OCT based on the dual graphics processing units architecture for microsurgery guidance. *Biomed Opt Express*. 2011;2:764–770.
108. Zhang K, Kang JU. Real-time 4D signal processing and visualization using graphics processing unit on a regular nonlinear-k Fourier-domain OCT system. *Opt Express*. 2010;18:11772–11784.
109. Kang JU, Huang Y, Zhang K, et al. Real-time three-dimensional Fourier-domain optical coherence tomography video image guided microsurgeries. *J Biomed Opt*. 2012;17:081403–1.
110. Klein T, Wieser W, Reznicek L, Neubauer A, Kampik A, Huber R. Multi-MHz retinal OCT. *Biomed Opt Express*. 2013;4:1890–1908.
111. Xu J, Wei X, Yu L, et al. High-performance multi-megahertz optical coherence tomography based on amplified optical time-stretch. *Biomed Opt Express*. 2015;6:1340–1350.
112. Yasuno Y, Hong Y, Makita S, et al. In vivo high-contrast imaging of deep posterior eye by 1-micron swept source optical coherence tomography and scattering optical coherence angiography. *Opt Express*. 2007;15:6121–6139.
113. Esmaeelpour M, Povazay B, Hermann B, et al. Three-dimensional 1060-nm OCT: choroidal thickness maps in normal subjects and improved posterior segment visualiza-

tion in cataract patients. *Invest Ophthalmol Vis Sci*. 2010;51: 5260–5266.

114. Pasricha ND, Shieh C, Carrasco-Zevallos OM, et al. Real-time microscope-integrated OCT to improve visualization in DSAEK for advanced bullous keratopathy. *Cornea*. 2015;34: 1606–1610.
115. Wong SC, Lee TC, Heier JS, Ho AC. Endoscopic vitrectomy. *Curr Opin Ophthalmol*. 2014;25:195–206.
116. Zeiss Cirrus HD-OCT technical specifications. Carl Zeiss Meditec, Inc. website. Available at: http://www.zeiss.com/meditec/en_us/products—solutions/ophthalmology-optometry/glaucoma/diagnostics/optical-coherence-thomography/oct-optical-coherence-tomography/cirrus-hd-oct.html#specifications. Accessed April 18, 2016.
117. Zeiss RESCAN 700 technical specifications. Carl Zeiss Meditec, Inc. website. Available at: http://www.zeiss.com/meditec/en_us/products—solutions/ophthalmology-optometry/glaucoma/therapy/surgical-microscopes/opmi-lumera-700.html#technical-data. Accessed April 18, 2016.
118. Steven P, Le Blanc C, Velten K, et al. Optimizing descemet membrane endothelial keratoplasty using intraoperative optical coherence tomography. *JAMA Ophthalmol*. 2013; 131:1135–1142.
119. Haag-Streit Surgical iOCT product description. Haag-Streit Surgical website. Available at: http://www.haag-streit-surgical.com/products/ophthalmology/ioctr.html. Accessed April 18, 2016.
120. Leica Microsystems EnFocus technical specifications. Leica Microsystems website. Available at: http://www.leica-microsystems.com/products/optical-coherence-tomography-oct/details/product/enfocus/. Accessed April 18, 2016.
121. Ferguson RD, Hammer DX, Paunescu LA, Beaton S, Schuman JS. Tracking optical coherence tomography. *Opt Lett*. 2004; 29:2139–2141.
122. Kocaoglu OP, Ferguson RD, Jonnal RS, et al. Adaptive optics optical coherence tomography with dynamic retinal tracking. *Biomed Opt Express*. 2014;5:2262–2284.
123. Sznitman R, Richa R, Taylor RH, Jedynak B, Hager GD. Unified detection and tracking of instruments during retinal microsurgery. *IEEE Trans Pattern Anal Mach Intell*. 2013;35: 1263–1273.
124. Li Y, Chen C, Huang X, Huang J. Instrument tracking via online learning. In: *Medical Image Computing and Computer-Assisted Intervention*: MICCAI 2014. Vol 17. 2014; 464–471.